Article

Soil Contaminated with Hazardous Waste Materials at Rio Tinto Mine (Spain) Is a Persistent Secondary Source of Acid and Heavy Metals to the Environment

Sandra Fernández-Landero [1], Juan Carlos Fernández-Caliani [1,*], María Inmaculada Giráldez [2], Emilio Morales [2], Cinta Barba-Brioso [3] and Isabel González [3]

[1] Department Earth Sciences, University of Huelva, 21071 Huelva, Spain; sandra.fernandez@dct.uhu.es
[2] Department Chemistry, University of Huelva, 21071 Huelva, Spain; giraldez@uhu.es (M.I.G.); albornoz@uhu.es (E.M.)
[3] Department Crystallography, Mineralogy and Agricultural Chemistry, University of Seville, 41071 Seville, Spain; cbarba@us.es (C.B.-B.); igonza@us.es (I.G.)
* Correspondence: caliani@uhu.es

Abstract: Mineralogical analysis and laboratory-based leaching tests coupled with speciation modeling were undertaken to quantify the potential for short-term acid generation and the release of trace elements from soils heavily contaminated with mine waste at Rio Tinto. Three different waste materials were considered as case studies: roasted pyrite, copper slags, and leached sulfide ores. The results showed elevated values of net acid generation (up to 663 mmol H^+/kg), the major pools being potential sulfidic acidity and acidity retained in jarosite. Remarkable contents of As and toxic heavy metals were found especially in the slag-contaminated soil. Copper, Zn, and Pb were the most abundant metals in the acid leach solutions resulting from mine soil-water interaction, with peak values of 55.6 mg L^{-1}, 2.77 mg L^{-1}, and 2.62 mg L^{-1}, respectively. Despite the high total contents of trace elements occurring in soil, the mobile fraction was limited to maximum release values of 12.60% for Cd and 10.27% for Cu, according to the test leaching. Speciation calculations indicated that free metal ions (M^{2+}) and sulfate species (MSO_4^0) accounted for most of the dissolved load. Acid soil drainage is a secondary source of acid and heavy metals in the mine site and, therefore, an effective land reclamation program should ensure that acidity and metal mobility are reduced to environmentally sustainable levels.

Keywords: Technosol; mine wastes; soil contamination; acidity; leaching test; metal release; speciation; ICP-OES/MS; acid soil drainage; Iberian Pyrite Belt

1. Introduction

Soil is a vital and non-renewable resource that is increasingly under pressure from a range of human activities, with mining being one of the leading anthropogenic forces driving environmental degradation. Acid generation and metal release from the oxidative dissolution of sulfide minerals in mine wastes is a well-documented issue in many historic mining districts [1–3]. Acid mine drainage (AMD) and heavy metal-bearing mineral particles arising from abandoned mine lands may pose a serious threat to human health and ecosystems [4–8]. Hence, a great deal of work has been undertaken to characterize the mineralogy, geochemistry, and environmental impacts of mine wastes [9–13]. However, there are still gaps in the research on mining-affected soil systems that need to be addressed.

The pollutants enter surrounding soils by seepage and run-off from mine wastes, AMD discharges, and atmospheric fallout, resulting in a legacy of mine-related anthropogenic soils that can be classified as Technosols according to IUSS Working Group WRB [14]. Mine Technosols contaminated with waste materials may have lost their natural resilience and adaptive capacity to retain harmful contaminants and, therefore, can generate acidic

effluents and release sulfate and potentially toxic elements (PTEs) into surface and pore waters [15]. This can be referred to as acid soil drainage (ASD) in analogy to AMD. Soil erosion and leaching are intensive during rain events leading to the dispersion of PTEs, either bound to suspended particles or as dissolved species. Knowledge of ASD is important for understanding the mobility and environmental availability of PTEs at historically contaminated sites, and also for developing sustainable remediation options to reduce the dispersion of contaminants and their associated risks [16]. Accurate prediction of ASD is challenging but essential to minimize the environmental impact of these soils.

The goal of this work was to assess the potential mobilization of acid and PTEs from mine Technosols contaminated with various types of mining and metallurgical wastes in the mining district of Rio Tinto (Spain). These drastically disturbed mine soils have been subjected to chemical loading for over two centuries in the absence of legal and regulatory frameworks. The sources and relative contributions of acid and PTEs from the mine Technosols are currently not well understood. Thus, the specific objectives of the study were: (1) to quantify the existing acidity and to predict the acid-forming potential from sulfide oxidation, and (2) to determine the element concentrations leached from the mine soils and then to evaluate the mobility of PTEs and their contribution for water pollution.

2. Site Description and Historical Background

Rio Tinto mine, located in Huelva province, Spain (Figure 1), is an internationally renowned mine not only for the giant size of its ore body but also because of its long history of mining and extractive metallurgy, dating back to pre-Roman times. It is the largest of the volcanogenic massive sulfide (VMS) deposits of the Iberian Pyrite Belt (IPB), with over 500 million tons of VMS ores averaging 45 wt.% S, 40 wt.% Fe, 0.8 wt.% Cu, 2.1 wt.% Zn, 0.8 wt.% Pb, 0.5 g/t Au, and 26 g/t Ag [17], and about 2 billion tons of low-grade stockwork mineralization including zones of economic copper ore (186 million tons at 0.38 wt.% Cu according to Noble [18]) that are currently being mined at Cerro Colorado open pit. Previous research on the geology and metallogeny of the Rio Tinto VMS deposit has been described in detail recently ([19] and references therein).
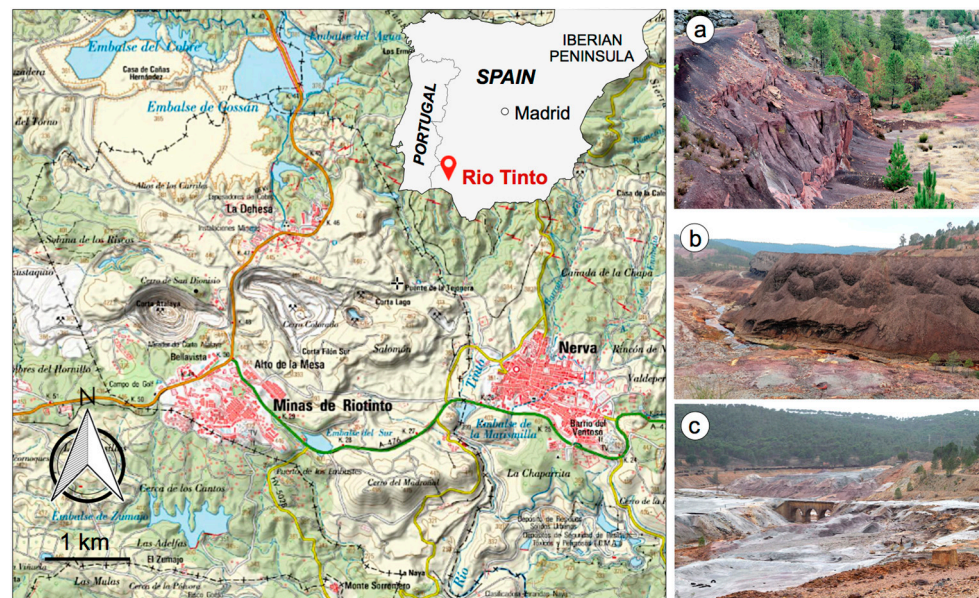

Figure 1. Location map of the Rio Tinto mining area (viewfinder SIGPAC), and representative photographs of the extensive mine wastes: (**a**) roasted pyrite piles; (**b**) slag dumps; and (**c**) heap leaching grounds (photo A. Delgado).

The Rio Tinto mining area is also an example of large-scale environmental degradation caused by long-lasting mining, ore processing, and smelting activities. It is generally accepted that Rio Tinto was extensively mined since at least the Late Bronze Age [20], being a major source of copper, gold, and silver in the Roman era, as evidenced by a large number of ancient slags widespread in the area (about 6 million tons according to Rothenberg and García-Palomero [21]).

Modern mining started in the middle of the 19th century with the extraction of cupreous pyrites, and major technological changes took place involving the smelting of high-grade ores in blast furnaces and converters. Slags produced during smelting were accumulated in significant amounts over time. Further details of the smelting works are given in Salkield [22]. The low-grade copper ores that were deemed unsuitable for smelting were converted into water-soluble sulfates by open-air roasting in heaps locally known as teleras. The roasted mineral (i.e., pyrite ash) was washed with acidic water to leach out the soluble metal-sulfate salts, leaving a solid residue enriched in ferric iron (red waste), while the leach liquors were conducted into cementation tanks where dissolved copper was precipitated by iron scrap chips. The red wastes resulting from that ancient process can be found today at the Planes and Peña de Hierro sites (Figure 1a).

In 1873 the British Rio Tinto Company (RTC) was formed to operate the mines and the scale of the operations was dramatically increased. The ore body was extensively worked from several open-pit and underground mines, focusing on copper-rich ores and massive pyrite for the manufacture of sulfuric acid. During the period of RTC operations (1873–1954), the total output of pyrite ores was almost 110 million tons [22]. The pyrite concentrates were transported by railway to Huelva port causing adverse impacts on the local soil environment due to hazardous cargo spills [23]. Pyrite smelting operated until 1970 to melt massive sulfide concentrates to produce blister copper, and at the same time to recover the excess sulfur in the elemental form. The smelting operations produced a vast volume of slag (at least 10 million tons with an average grade of 0.44 wt.% Cu according to Lottermoser [24]) placed along the banks of the Tinto River, in the industrial complex of Zarandas (Figure 1b).

Heap leaching was another widely used extraction method for low-grade ores since the early 20th century. An average of about 2000 tons of ore per day was delivered from the mines to the heaps by railway wagons, with La Naya becoming the main center of operations (Figure 1c). In more recent times, high-grade copper stockwork mineralization and gold-bearing gossan, which overlies the VMS deposit, were exploited by opencast mining. The Rio Tinto mine was last operated in 2001 and restarted operations in 2015 owing to the rise in the copper price. The current open pit mining operation is focused on the Cerro Colorado deposit, including Filón Sur and Filón Norte orebodies.

Extensive opencast workings and smelting activities as well as the lack of environmental protection have resulted in land contamination arising from past waste disposal practices. The natural soil was irreversibly damaged or transformed into degraded land unable to support plant life over a bare area of about 1000 ha (Figure 2). Huge quantities of mine and metallurgical wastes, including sulfide-rich waste dumps, ore stockpiles, slag deposits, roasted pyrite residues, heap leaching grounds, and tailings impoundments were left without any environmental control. These hazardous materials have the potential for releasing a variety of dissolved metals and metalloids that are usually present in the ores as minor or trace elements, such as Cu, Pb, Zn, As, Cd, Sb, and Tl, thus causing serious environmental pollution to the surrounding soils and vegetation [25–30].
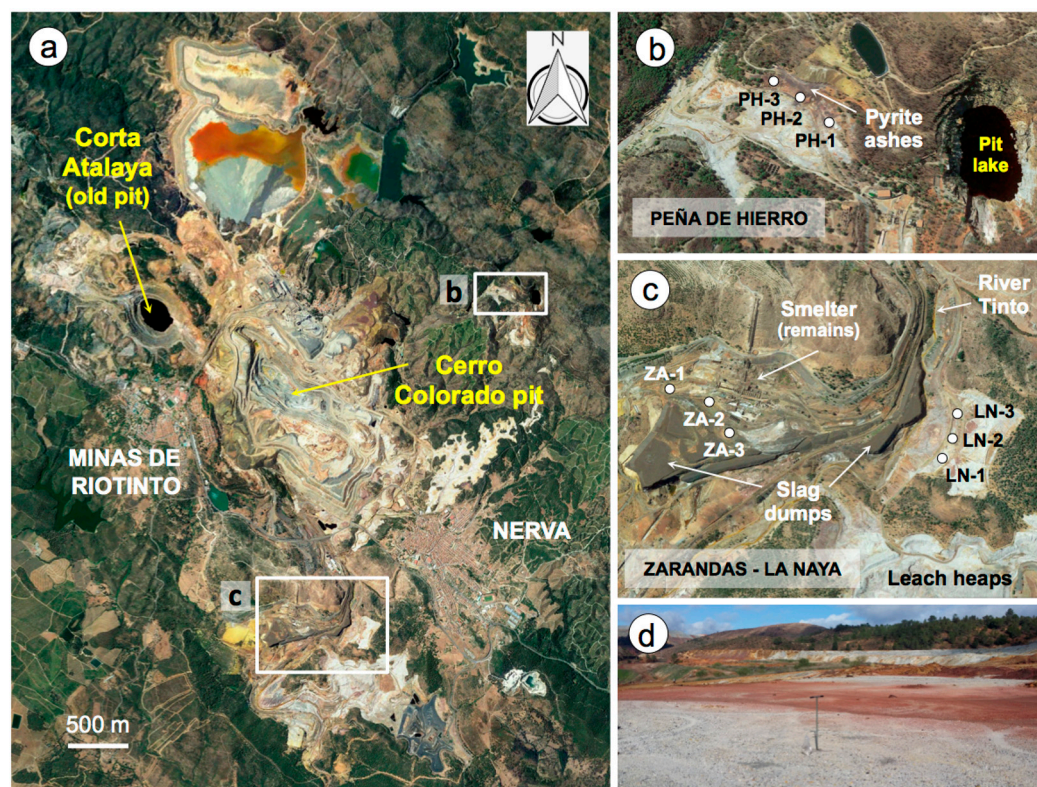
Figure 2. Satellite view (Google Earth) of the Rio Tinto copper mine showing: the mining-affected area (**a**); the location of the sampling sites at Peña de Hierro (**b**) and Zarandas-La Naya (**c**); and the method for taking soil samples with hand auger (**d**).

3. Materials and Methods

3.1. Sample Selection and Preparation

Three different Technosols containing abundant artifacts in the form of mine waste particles were selected for this study: (1) Technosol contaminated with roasted pyrite wastes from the Peña de Hierro mine site (hereafter referred to as PH; Figure 2b); (2) Technosol contaminated with copper slags from the old smelter *Fundición Piritas* at Zarandas (hereafter referred to as ZA; Figure 2c); and (3) Technosol contaminated with leached sulfide ores from the leach heap grounds of La Naya (hereafter referred to as LN; Figure 2c). These areas have experienced considerable environmental damage and were selected on the basis of being representative of mine-related anthropogenic soils in the mining district of Rio Tinto.

Within each selected area, soil samples were collected with an Edelman hand auger from the surface layer (0–20 cm) at three randomly selected sites and stored in airtight polyethylene bags. At each sampling site, a composite sample of about 10 kg was obtained by bulking five topsoil samples taken in crossing directions and spaced approximately 1.5 m around the central point (Figure 2d). The composite samples were thoroughly mixed to ensure optimal homogenization, dried at room temperature ($20 \pm 1\ ^\circ$C), gently disaggregated, and sieved to 2 mm. A portion of the sieved sample was ground in an agate mortar and passed through a 63 μm sieve for analysis.

3.2. Soil Characterization Methods

Soil reaction (pH), redox potential (Eh), and electrical conductivity (EC) were determined by stirring 10 g of soil in 25 mL of deionized water, after shaking for 5 min, and left to stand for 30 min. Soil pH was also determined in 1 M KCl suspension at the soil-to-solution ratio of 1:2.5 (m/v), and in a suspension of soil after digestion by 30% hydrogen peroxide (H_2O_2) in a 1:20 (m/v) soil-to-solution ratio [31]. The reaction was allowed to continue until the bubbling stopped (about 6 h after the addition of H_2O_2). The pH values in water

(pH_{H2O}), KCl (pH_{KCl}), and H_2O_2 (pH_{ox}) suspensions were measured with a digital pH meter properly calibrated with two buffer solutions at pH 4 and 7. All measurements were performed in triplicate and averaged.

Mineralogical analysis of the bulk sample was performed by X-ray diffraction (XRD) with a BRUKER AXS D8-Advance powder diffractometer (CITIUS, University of Seville) using monochromatic Cu-Kα radiation. The instrument was operated under standard conditions: 40 kV voltage and 30 mA current in the angular range of 3–70° 2θ with a step size of 0.015° and a scan speed of 0.1 s per step. Intensity factors weighting integrated peak area values of diagnostic reflections in combination with the 100% approach [32] were applied to obtain semiquantitative mineral abundances.

To assist in the identification of metal-bearing accessory minerals and poorly crystallized phases, the samples were coated with a thin layer of sputtered carbon and examined by field-emission scanning electron microscopy (FESEM) with a JEOL JSM-IT500HR instrument (University of Huelva) fitted with an energy dispersive X-ray spectroscopy (EDS) detector (Oxford Instruments). The samples were observed in both secondary electron (SE) and backscattered electron (BSE) modes. The working distance was set at 10 mm, accelerating voltage at 20 kV, and probe current at 2.5 nA.

Quantitative analysis of the elemental composition of selected phases was conducted on polished sections by electron probe microanalysis (EPMA) using a JEOL JXA-8200 SuperProbe (University of Huelva) equipped with four wavelength dispersive X-ray spectrometers. The instrumental operating conditions were accelerating voltage at 20 kV, beam current at 20 nA, and beam diameter up to 5 μm allowing point-by-point element determination. A set of synthetic materials and well-characterized minerals was used as standards for calibration.

The composite bulk soil samples were analyzed for the determination of the total contents of PTEs of environmental significance (As, Cd, Co, Cr, Cu, Ni, Pb, Sb, Tl, and Zn). First, a 0.25 g sample was digested with four acids beginning with HF, followed by a mixture of HNO_3 and $HClO_4$, and then heated in several ramping and holding cycles. After incipient dryness was attained, samples were brought back into the solution using aqua regia. The analysis was conducted by inductively coupled plasma optical emission spectrometry (ICP-OES) with an Agilent 735 instrument at Activation Laboratories (Ancaster, ON, Canada), which is accredited to ISO 9001 and ISO/IEC 17,025 standards. ICP-OES has a proven history as an appropriate tool to assess metal contamination [33].

Quality control of the analytical method included the use of reagent blanks, replicate analysis of two samples, and a range of certified reference materials (OREAS 13b, OREAS 98, OREAS 101b). Analysis of the reference materials yields values that deviated from the certified contents by less than 10% (relative standard deviation, RSD). Reproducibility of the analytical data was better than 2% RSD for most of the elements reported and always better than 5% RSD.

3.3. Static Test Methods

Acid-forming potential (net acidity) was quantified for acid soil drainage prediction using an acid-base accounting (ABA) approach that involves determining the total acid-generating capacity and the acid-neutralizing capacity of the soils. In the context of acid sulfate soils, the total acid-generating capacity comprises the potential sulfidic acidity in addition to the existing acidity, which in turn includes actual (soluble plus exchangeable) and retained acidity [34]. Thus, the global ABA equation can be expressed in the following form: Net acidity = Potential sulfidic acidity + actual acidity + retained acidity − acid neutralizing capacity.

Potential sulfidic acidity (PSA) was determined by measuring the pyrite sulfur (S_{pyr}) extracted with 6 M HNO_3 solution heated at 120 °C for 30 min, performed on the residue remaining after sulfate extraction with hot dilute HCl acid, according to the standard test method ASTM D2492-02 optimized for Fe-rich soils. The S_{pyr} concentration of the extract was analyzed by ICP-OES using an Agilent 5110 instrument (University of Huelva,

Supplementary Table S1), and then used to calculate the potential pool of sulfidic acidity. The weight percent of S_{pyr} was multiplied by the stoichiometric factor of 625 to give the PSA value in mmol H^+/kg, based on the theoretical assumption that each mole of pyrite releases two moles of sulfuric acid [35,36].

Acidity existing in the soil as a consequence of previous sulfide oxidation, resulting either from the dissolution of readily soluble sulfates (actual acidity) or from acid adsorbed onto negative exchange sites of the soil particles (exchangeable acidity), was measured directly by titrating a 1 M KCl soil suspension with 0.1 M NaOH to a pH endpoint of 7.0 [37]. Additional existing acidity stored in sparingly soluble hydroxy-sulfate minerals, particularly jarosite (a conspicuous product of pyrite oxidation), was calculated from the concentration of sulfate sulfur (S_{jar}) extracted with a 0.2 M NH_4-oxalate solution adjusted to pH 3.0 and heated at 80 °C for 2 h [38]. The extract solutions were analyzed for S_{jar} using the Agilent 5110 ICP-OES. The weight percent of NH_4-oxalate extracted sulfur was multiplied by the stoichiometric factor of 468 to convert the S_{jar} values to equivalent acidity units (mmol H^+/kg) on the basis that one mole of sulfur in jarosite releases 1.5 moles of acidity.

Alternatively, a direct approach to give an indication of acid-forming potential was made for measuring net acid generation (NAG) using an H_2O_2-based static test. For the NAG test, 2 g of dry soil was treated with 40 mL of 30% H_2O_2 to accelerate the oxidation of pyrite, followed by measurement of the pH of the extract solution and titration with 0.1 M NaOH until pH 7 was reached, thus allowing the product to react with the acid-neutralizing minerals, if any.

3.4. Leaching Test

The leaching test was performed according to European Standard EN-12457-4 [39] in order to determine the element concentrations leached from the mine Technosols, and then to assess the mobility of PTEs and their potential impact on water resources.

Following this test procedure (Figure 3), a dry mass of soil was placed in contact with distilled water under a liquid-to-solid (L/S) ratio of 10 L kg^{-1}, and kept under agitation for 24 h. The solid residue was separated by filtration using a 0.45 μm membrane filter, and the PTE concentrations (As, Cd, Cr, Cu, Ni, Pb, and Zn) in the leachates were analyzed by inductively coupled plasma mass spectrometry (ICP-MS) using an Agilent 7700 instrument (University of Huelva, Supplementary Table S1). Multi-element standard-2A Agilent solutions were used for external calibration, and 10 μg L^{-1} of Ge, Rh, Sc, and Tb were used as internal standards. The accuracy and reproducibility of the analytical data were better than 10% RSD for most analyzed elements.
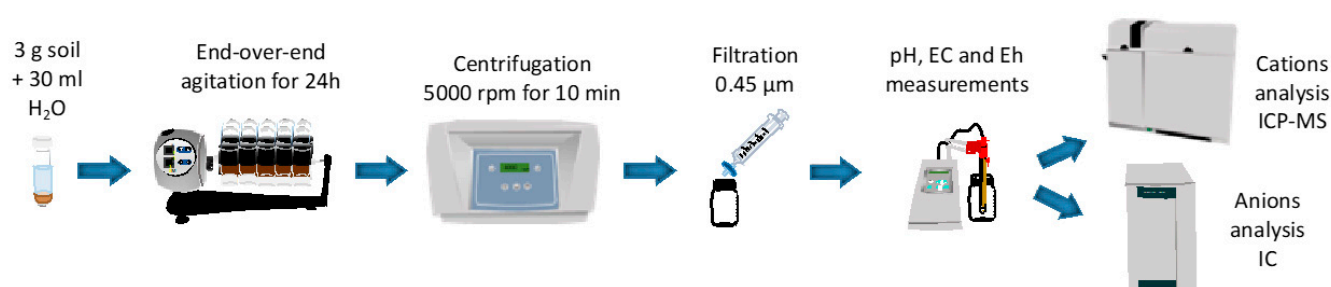

Figure 3. Simplified flow diagram of the static leaching test.

The eluate solution recovered from the leaching test was also analyzed for sulfate, nitrate, and chloride anions by ion chromatography with a Metrohm 883 Basic IC plus instrument (University of Huelva), and the leaching conditions were recorded in terms of pH, electrical conductivity and redox potential (Eh) values.

4. Results and Discussion

4.1. Soil Components with Emphasis on Heavy Metal-Bearing Particles

Combined results from XRD and FESEM-EDS analysis of the bulk fraction (<2 mm) revealed that the mine soils impacted by waste materials have a contrasting mineral composition (Table 1). The chemical composition of randomly selected heavy metal-bearing particles obtained from EPMA is also listed in Table 1.

The soil contaminated with roasted pyrite wastes (PH) is mineralogically composed of well-crystalized iron oxides (hematite), jarosite, and quartz, with subordinate amounts of phyllosilicates (mica and kaolinite), feldspars, and barite. Hematite is responsible for the distinctive weak red color (Munsell 10R 4/2) of this Technosol. The essential mineralogy is in line with that described in the literature for historic pyrite ash wastes of the Rio Tinto mining area [40,41]. The XRD patterns displayed a high background signal indicating the occurrence of amorphous or poorly ordered material in the PH samples. Moreover, the FESEM-EDS examination (Figure 4) allowed the identification of anglesite, often forming overgrowths on barite crystals, and confirmed the presence of abundant iron oxide aggregates with a porous texture (Figure 4a). EPMA analysis of representative hematite particles (Table 1) showed that they are almost chemically pure with only trace amounts (less than 0.5 wt.%) of Cu, As, Sb and S. The EPMA study also revealed Pb-rich barite veins filling pre-existing cracks within barite (Figure 4b).

Table 1. Mineral composition of the Technosols and EPMA analysis of selected mineral particles.

Technosol	Peña de Hierro (PH)					Zarandas (ZA)					La Naya (LN)			
Major minerals Accessories	Hem + Jrs + Qz Mca + Fsp + Brt + Ang					Mca + Chl/Kln + Qz ± Jrs ± Py Fsp + Brt ± Hem ± Jrs ± Gp					Qz + Py + Mca ± Jrs Fsp + Brt + Ang ± Jrs ± Hem ± Gp			
Oxides (wt.%)	Hem$_1$	Hem$_2$	Hem$_3$	Ang$_1$	Ang$_2$	Jarosite-like minerals				Ang	Jarosite-like minerals		Pb-rich phosphate	
Fe$_2$O$_3$	99.74	99.17	97.96			45.78	27.94	42.38	53.73		38.02	37.45	7.21	4.34
SO$_3$	0.05	0.03	0.03	25.60	27.05	17.93	14.01	23.44	21.97	26.17	23.66	22.88	5.29	4.48
As$_2$O$_5$		0.04				4.00	9.88	2.66	4.97		0.70	3.14	1.67	2.34
Sb$_2$O$_5$	0.04	0.05	0.02	0.05	0.05	0.15	3.55	0.20	0.11		0.34	0.44	0.07	0.13
P$_2$O$_5$													12.13	11.67
PbO				73.97	72.19	1.40	12.55	8.30	1.98	73.11	14.88	12.31	32.60	31.69
CuO	0.05	0.05	0.03			0.24	0.24	0.68	0.21		0.45	0.20	0.13	0.13
ZnO							0.06	0.06						
K$_2$O						1.24	0.53	1.19	1.40		1.54	3.68	0.39	0.41

Mineral abbreviations: Ang (anglesite); Brt (barite); Chl (chlorite); Fsp (feldspar); Gp (gypsum); Hem (hematite); Jrs (jarosite-like minerals); Kln (kaolinite); Mca (mica); Py (pyrite); Qz (quartz).

The slag-contaminated soil samples from Zarandas (ZA) are made up of quartz, phyllosilicates (mica, chlorite, and/or kaolinite), and feldspars along with variable quantities of jarosite (up to 25 wt.%) and accessory hematite, barite, and gypsum. This Technosol contains numerous copper slag fragments consisting of feathery crystals of fayalite with the interstices filled with glassy material (Figure 4c), in which tiny crystals of magnetite and more rarely matte particles and spherical copper nanoparticles are disseminated, as detected by FESEM-BSE-EDS (Figure 4d). The fayalitic slag often had a vesicular texture with jarosite-lined voids. In addition, the EDS spectra indicated the occurrence of As-bearing iron mineral particles attributable to amorphous ferric arsenate or scorodite, and complex phase mixtures containing S-Fe-Pb-As-(Cu)-(Sb). The results of EPMA analyses (Table 1) of selected micro-areas suggest that the chemical composition of such phases may be compatible with jarosite-like minerals (Pb-jarosite and Pb-As-jarosite) that appear mixed with iron oxides. Interestingly, the sample ZA-3 showed a strikingly high content of pyrite (20–25 wt.%), most likely sourced from sulfide ores used for manufacturing sulfuric acid in a plant adjacent to the smelter site. The presence of readily water-soluble sulfate salts in the slag-contaminated soil (Figure 5a) and the widespread occurrence of efflorescent sulfate minerals at seepage points of the slag dumps [24], support the idea that these metallurgical wastes are chemically active long after the mining period.
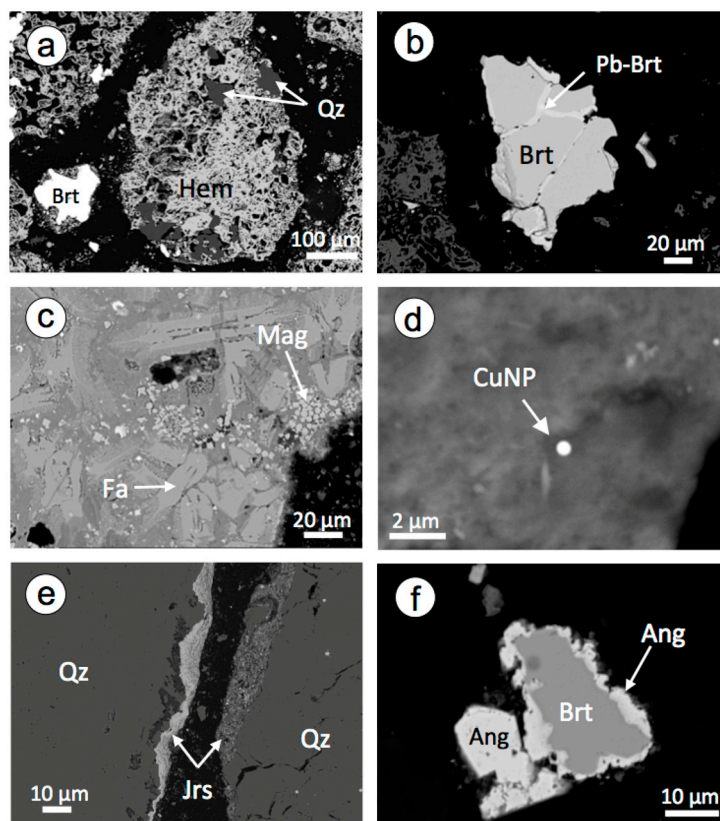
Figure 4. BSE images of polished sections showing in detail some textural and compositional features of the Technosols. (**a**) Aggregates of hematite (Hem) with inclusions of quartz (Qz) (sample PH-2); (**b**) Pb-rich barite (Pb-Brt) occurring as crack fillings in barite (sample PH-2); (**c**) slag artifact (sample ZA-1) composed of lath-shaped fayalite (Fa) and disseminated magnetite (Mag); (**d**) Copper nanoparticle (CuNP) embedded in the fine-grained matrix of the slag; (**e**) quartz (Qz) grains coated by Pb-As-bearing jarosite (Jrs) rims (sample LN-3); (**f**) Barite (Brt) crystals enclosed by anglesite (Ang) overgrowths (sample LN-3).
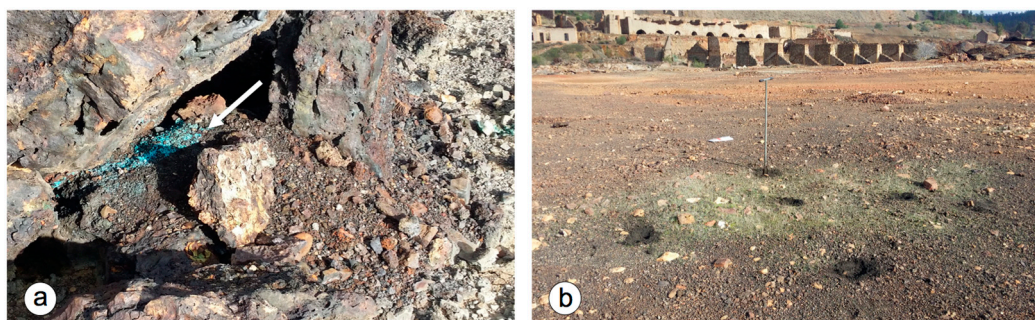

Figure 5. Field pictures of the Technosol ZA showing: (**a**) sulfate precipitate occurring as greenish blue efflorescence (white arrow) on the slag-contaminated soil; and (**b**) grass plants growing in the vicinity of the old smelter site on patches of soil with a moderately acid reaction.

The Technosol contaminated with leached ores from the heap leaching grounds of La Naya (LN) is comprised of mixtures of quartz, pyrite, mica, and jarosite-group minerals, with minor hematite, feldspars, barite, and anglesite. The FESEM-EDS study showed actively oxidizing crystals of pyrite with pitted surfaces. Jarosite was commonly found forming aggregates of euhedral pseudo-cubic crystals, but also appeared as coatings and rims covering grains of quartz or feldspars (Figure 4e). BSE images on polished sections revealed the occurrence of barite crystals enclosed by anglesite (Figure 4f). The jarosite-like

minerals contain significant amounts of Pb and As, and minor levels of Sb and Cu, as determined by EPMA analysis (Table 1), which also allowed us to infer the presence of Pb-rich phosphate particles with additional amounts of Fe, S, and As.

Therefore, the mining-affected soils are variable in mineral composition. Besides quartz, feldspars, and phyllosilicates, which are remnants of the original soil, a variety of heavy metal-bearing particles have been inferred as both primary contaminants of mine wastes (pyrite, hematite, copper slags) and secondary products of oxidation, dissolution, and precipitation reactions (jarosite-group minerals, amorphous iron oxyhydroxides, scorodite, anglesite, and gypsum). Overall, this mineral assemblage is consistent with the mineralogy of the alluvium contaminated by metal mining in the Rio Tinto area [16].

4.2. Total Acid Generating Capacity and Net Acidity

The soils of the areas under study were mostly extremely acidic in reaction when suspended in water, with pH_{H2O} values below 3.5, although the slag-contaminated soil samples (Technosol ZA) spanned a range of values between 3.0 and 5.4 (Table 2). A few patches of grass were seen at the site growing on the least acid soil (Figure 5b). They are all well aerated with Eh values consistently over +500 mV reflecting strongly oxidizing conditions. The soil electrical conductivity was always lower than 2 mS cm^{-1}, which is indicative of a relatively low soluble salt concentration in the soil solution. Similar results were obtained when the soil pH was measured in a 1M KCl solution (pH_{KCl} = 2.4–5.3), with the exception of the sample ZA-2 whose average pH_{KCl} value was 1.2 units lower than that measured in water. Nonetheless, the pH measured after complete oxidation of the sample with H_2O_2 varied noticeably among the different mine soils, depending on the relative abundance of pyrite. The lowest pH_{ox} levels (1.7–1.9) were found in the Technosol LN, where pyrite is a ubiquitous mineral, revealing a latent acid-generating capacity after sulfide oxidation. The Technosol PH showed pH_{ox} values close to those measured in water and KCl solution due to the lack or scarcity of sulfide minerals, while the pH_{ox} of the Technosol ZA varied between around 2.0 (samples ZA-1 and ZA-2) and 5.1 (sample ZA-3). However, it must be pointed out that the sample ZA-3 had a pH_{ox} of 3.0 after 2 min of contact with H_2O_2, indicating a likelihood of potential sulfidic acidity. Thus, all samples are potentially acid generating as the pH values after H_2O_2-reaction were less than 4.0 in the short term.

**Table 2.** Soil pH values, sulfur speciation, and major pools of acidity.

Sample	pH			Sulfur Speciation (wt.%)			Acidity (mmol H⁺/kg)				
	H₂O	KCl	H₂O₂	S$_{total}$	S$_{pyr}$	S$_{jar}$	PSA	TAA	RA	TAG	NAG
PH-1	2.96	3.00	2.83	2.60	0.18	1.71	111	90	800	1001	144
PH-2	2.51	2.57	2.45	2.75	0.15	0.78	93	27	367	487	104
PH-3	2.14	2.58	2.41	2.63	0.16	1.07	97	36	503	636	93
ZA-1	2.96	2.75	1.86	2.53	0.16	2.44	102	19	1146	1267	442
ZA-2	4.56	3.36	2.20	0.55	0.11	0.24	66	10	110	186	632
ZA-3	5.35	5.34	5.08	6.80	3.54	1.78	2214	7	835	3056	240
LN-1	2.68	2.49	1.85	2.97	2.00	0.32	1248	26	151	1425	663
LN-2	2.51	2.44	1.65	3.15	1.42	1.66	890	30	780	1700	609
LN-3	3.02	3.01	1.78	1.67	1.26	0.33	786	31	153	971	463

PSA (Potential Sulfidic Acidity); TAA (Titratable Actual Acidity); RA (Retained Acidity); TAG (Total Acid Generation); NAG (Net Acid Generation).

Even though pH is a primary index for soil acidity, it gives no indication of the total acid-generating capacity of the Technosols. The measurement of total sulfur (S$_{total}$) is an option widely used for estimating the maximum potential acidity from sulfide sources [34]. According to the S$_{total}$ content measured in soil (Table 2), the potential acid release should be in the range of 340–4250 mmol H⁺/kg. But this conservative approach overestimates the potential acid risk of the studied soils, in which a fraction of sulfur is in the form of jarosite and non-acid-producing sulfate minerals, such as gypsum and barite, and additionally,

no account is made for acid-neutralizing potential. This fact highlights the importance of quantifying the various pools of acidity in the mine soils (Table 2).

Among the acid-generating components of the soil, pyrite is by far the major contributor to acid production at the mine Technosols. As noted previously, no other sulfide minerals were detected in any sample. Based on the stoichiometry of pyrite oxidation, one mole of sulfur in pyrite produces two moles of protons through the reaction:

$$FeS_2 + {}^{15}/_4O_2 + {}^7/_2H_2O \rightarrow Fe(OH)_3 + 4H^+ + 2SO_4{}^{2-}$$
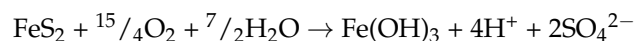
The content of S_{pyr} in the Technosol LN ranged from 1.26 to 2.00 wt.%, which is compatible with a latent acidity of 780–1250 mmol H^+/kg in soil, equivalent to a potential sulfidic acidity (PSA) of 38.6–61.2 kg H_2SO_4/t. Conversely, the S_{pyr} percent was quite low (0.15–0.18 wt.%) in the Technosol PH, confirming that very few remnants of unroasted sulfide ores were present in the soil contaminated with pyrite ashes. So, the latent acidity released from sulfide oxidation is expected to be consistently low (around 100 mmol H^+/kg equivalent to the production of 3.06 kg H_2SO_4/t). The acid-production capacity due to sulfide oxidation of the Technosol ZA varied from sample to sample, reaching a maximum of 2210 mmol H^+/kg (about 108 kg H_2SO_4/t) in the sample ZA-3 due to its high content of pyrite (S_{pyr} = 3.54 wt.%). The samples ZA-1 and ZA-2 showed a latent acidity (3.4–4.9 kg H_2SO_4/t) considerably lower than the median acid producing potential (47.5 kg H_2SO_4/t) of the Zarandas slag deposit [24].

Soluble and exchangeable acidity existing in the soil as a consequence of previous oxidation of pyrite was relatively low, with mean values of titratable actual acidity (TAA) ranging from 12 mmol H^+/kg (Technosol ZA) to 51 mmol H^+/kg (Technosol PH). These findings are indicative that acidic conditions resulting from either dissolution of readily soluble sulfates (actual acidity), or acid adsorbed at the exchange sites of the soil particles (replaceable acidity), are limited. The eventual occurrence of soluble sulfate salts is likely to be an instantaneous source of acidity upon dissolution [42], and the presence of exchangeable and soluble Al species may be also an additional component of the existing acidity [37].

It is noteworthy that the oxidation of pyrite did not reach completion. The mine soils contain actively oxidizing crystals of pyrite in variable amounts, and their oxidation products other than iron oxy-hydroxides and sulfuric acid were and are being formed, such as poorly soluble iron hydroxy sulfate minerals. In fact, a portion of the sulfate ions and acid generated by pyrite oxidation appears to be stored in jarosite-like minerals, which are a major source of retained acidity under the oxidizing and acidic (pH < 3.5) conditions prevailing in the mine soils, where they are present in substantial amounts. The retained acidity values were within the ranges of 360–800 mmol H^+/kg (Technosol PH), 110–1150 mmol H^+/kg (Technosol ZA), and 150–780 mmol H^+/kg (Technosol LN) on the basis of the content of S_{jar} in soil samples. This retained acidity (RA) represents the less available form of the existing acidity that may be slowly released over time by hydrolysis of jarosite-like minerals [34], assuming that one mole of sulfur in jarosite would produce 1.5 moles of protons through the reaction:

$$KFe_3(SO_4)_2(OH)_6 + 3H_2O \rightarrow K^+ + 3Fe(OH)_3 + 2SO^{2-} + 3H^+$$

Thus, the total acid generating (TAG) capacity of the Technosols, comprising potential sulfidic acidity and existing acidity (i.e., soluble plus exchangeable and retained acidity) showed the following order of increasing acidity expressed in mmol H^+/kg: Technosol PH (710) < Technosol $ZA_{SAMPLES\ 1-2}$ (730) < Technosol LN (1360) < Technosol $ZA_{SAMPLE\ 3}$ (3060). The potential sulfidic acidity of the Technosol LN and Technosol ZA (sampling site ZA-3) accounted for 71% and 73% of TAG, respectively. The acidity retained in jarosite was the dominant acidity pool in the Technosol PH and Technosol ZA (sampling sites ZA-1 and ZA-2), comprising 79%–86% of TAG, respectively, while actual acidity accounted for less than 7% (Figure 6).
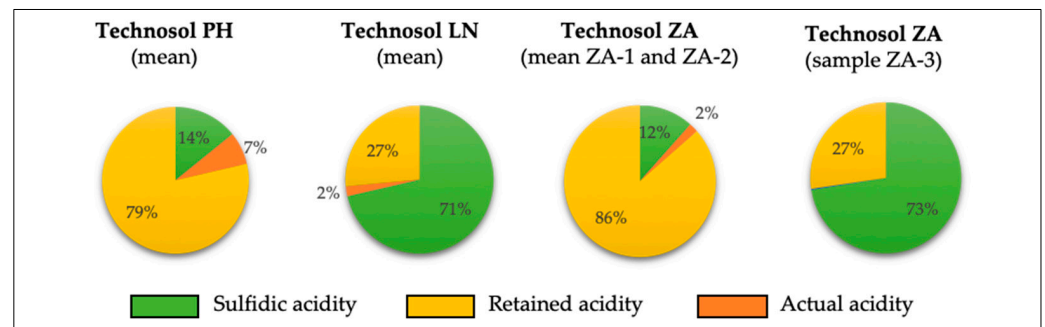
Figure 6. Pie charts comparing the percentage distribution of sulfidic, retained, and actual acidity in the Technosols.

The Technosols have a low buffering capacity to neutralize the amount of acid that is being produced, or has been produced, given the lack of carbonates and other reactive acid-neutralizing minerals. Certainly, the results from an H_2O_2-based static test (Table 2) suggest that the sulfidic acidity is unable to be neutralized by potential acid-consuming phases, as shown by the following mean values of net acid generation (NAG): 114 mmol H^+/kg (Technosol PH), 438 mmol H^+/kg (Technosol ZA) and 578 mmol H^+/kg (Technosol LN). It should be noted that these figures are an estimate of the acidity in the surface 20 cm only, and the NAG values provide a direct measure of the net amount of acid produced by the soil assuming that acid generation and acid neutralization reactions occur simultaneously [43,44]. The occurrence of labile or existing acidity is another indication that the acid-neutralizing capacity of the mine soils seems to be not effective [37].

4.3. Heavy Metal Contamination

The total contents of PTEs in the mine soil samples are listed in Table 3, including those below the detection limit and over-range values. For comparative purposes, Table 3 also provides PTE contents compiled from the literature for mine wastes of the Rio Tinto mining area, pedogeochemical baseline levels, and reference values for PTEs in soils around the abandoned mines of the IPB.

Trace element geochemistry of the Technosols is clearly dominated by chalcophile elements, with Cu, Pb, As and Zn being the major contributors to the heavy metal budget. Unusually high contents of Cu (>10,000 mg kg^{-1}), Pb (>5000 mg kg^{-1}), As (>5000 mg kg^{-1}), and Zn (up to 3810 mg kg^{-1}) were measured in some slag-contaminated soil samples. It was found that the Pb content also exceeded 5000 mg kg^{-1} in all Technosol LN samples. These levels are more than two orders of magnitude above the regional baseline values, and they are comparable, or even higher, than those reported for mine wastes in the reference sites [24,40,41,45], as well as in other severely polluted mine soils of the IPB [27] and elsewhere in the world [46,47].

Furthermore, the contents of Bi (up to 260 mg kg^{-1}), Tl (up to 81 mg kg^{-1}), Sb (up to 42 mg kg^{-1}), and Cd (up to 28 mg kg^{-1}) were higher than those reported in the literature for natural soils and sediments [48]. In contrast to the chalcophile elements, the contents of Cr, Ni, and Co in most samples were found to be within, or slightly above, the typical range of the regional soils, indicating that they are naturally occurring. However, some contamination was found at the sampling site ZA-3, where the Co content was over 7-fold higher than the baseline level.

As evidenced from the results of mineral characterization, a considerable amount of PTEs seems to be bonded to secondary phases, such as jarosite-group minerals, iron oxyhydroxides, anglesite, and Pb-rich phosphate, which would have scavenged contaminants from the soil solution, notably Pb and As, through structural incorporation, surface adsorption or co-precipitation mechanisms. Jarosite minerals also likely served as a secondary host of Tl, as described in mine soils and AMD systems elsewhere [40,49]. Altogether, the above findings support the claim that soil acted not only as a storage for heavy metal-bearing

particles (pyrite, hematite, fayalitic slag, etc.) eroded from the wasteland, but also as a geochemical sink for PTEs released into solution by sulfide oxidation. The content of Cu in the Technosol ZA was between 50 and 300 times higher compared to the background. This abnormally high Cu content could be reasonably explained by the occurrence of slag fragments with entrapped matte particles that represent the copper loss in the slag during the smelting process.

Table 3. Chemical composition of trace elements measured in the bulk soil samples (<2 mm) by ICP-OES and reference values reported for comparison.

Element (mg kg^{-1})	As	Bi	Cd	Co	Cr	Cu	Ni	Pb	Sb	Tl	Zn
Detection Limit	3	2	0.3	1	1	1	1	3	5	5	1
Technosol PH											
PH-1	319	86	3.0	46	18	504	8	2340	<5	12	415
PH-2	150	108	3.3	46	7	400	8	3420	19	17	314
PH-3	152	100	3.1	47	9	384	9	2980	19	15	311
Roasted pyrite wastes (mean)											
Peña de Hierro [1] (N = 3)	665		2.3	36	21	474	11	2707			561
Planes [2] (N = 3)	1026					338		4515		70	267
Technosol ZA											
ZA-1	>5000	121	4.9	15	67	1660	24	>5000	42	81	576
ZA-2	532	20	1.0	43	89	4370	70	1850	11	<5	1790
ZA-3	3630	174	27.8	142	149	>10,000	101	>5000	24	16	3810
Copper slag wastes (mean)											
Zarandas [3] (N = 6)	110	5.6	4.5	283		4410	17	2088	380	5.5	
Technosol LN											
LN-1	868	133	1.7	12	21	939	5	>5000	6	15	655
LN-2	2030	260	1.7	7	31	178	5	>5000	7	56	400
LN-3	1040	116	1.1	8	14	199	6	>5000	<5	9	266
Heap leaching wastes											
Rio Tinto [4]	4310		0.7	25	77	537	11	7056	765	9	478
Reference values											
Regional geochemical baseline [5]	25			19	95	32	35	38			76
Mine soils of Iberian Pyrite Belt [6]	361		0.7	15	78	412	19	1080			298

Data source: [1] [40]; [2] [41]; [3] [24]; [4] [45]; [5] [50]; [6] [51].

Based on calculation methods that relate the total contents of PTEs in soil and their regional baseline levels, an estimation of the extent of multi-element contamination was made by taking the four highest enriched elements (As, Cu, Pb, and Zn) and using the following formula [52]:

$$C_d = \sum_{i=1}^{n} C_f^i$$

where C_d is the contamination degree, *n* is the number of considered elements (*n* = 4 in this study), and C_f is the contamination factor for a given element (*i*), which is defined as the quotient between the PTE content measured in the soil (C_s) and the regional baseline (C_b), as follows:

$$C_f = \frac{C_s}{C_b}$$

The mean C_f values of the four elements of concern were in the following descending order: Pb $\gg$ Cu > As > Zn for Technosol PH; Cu > Pb > As $\gg$ Zn for Technosol ZA; and Pb $\gg$ As $\gg$ Cu > Zn for Technosol LN.

The pollution load index (PLI) of Tomlinson [53] was also used to calculate the degree of soil contamination as a geometric mean of C_f values based on the following formula:

$$PLI = \left(C_{f_{As}} \times C_{f_{Cu}} \times C_{f_{Pb}} \times C_{f_{Zn}} \right)^{1/4}$$

The results showed that all samples of the Technosols ZA and LN were found to be ultra-high contaminated, with ZA-3 ($C_d = 639$) and ZA-1 ($C_d = 391$) being the most contaminated sampling sites (Figure 7), whereas the samples of the Technosol PH ($C_d = 96$–113) showed extremely high contamination, according to the descriptive classes of soil contamination [54]. Consistently, the PLI values ranged widely from 12 (samples PH-2 and PH-3) to a maximum of 132 (sample ZA-3).
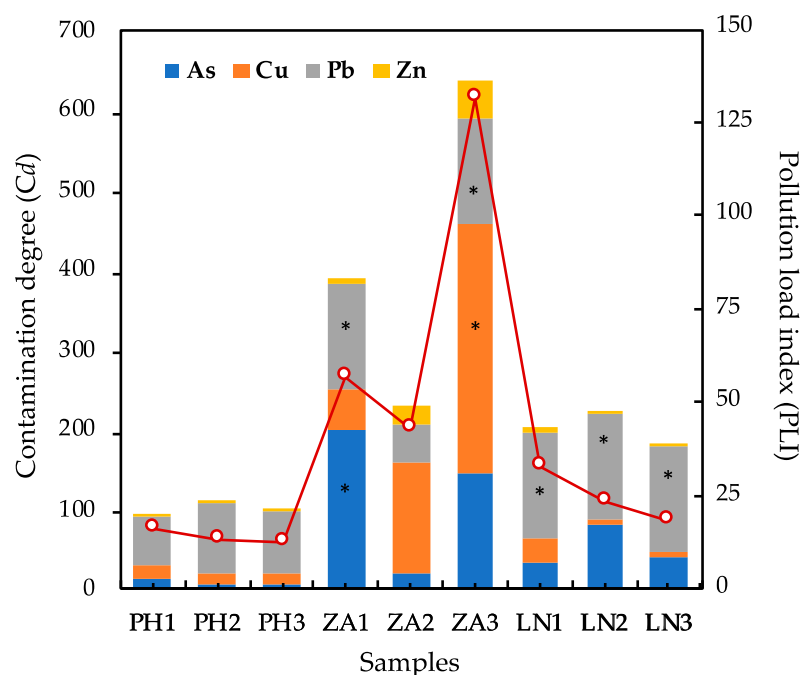

Figure 7. Combined bar and line chart showing the contamination degree (C_d) and the pollution load index (PLI) values, respectively. The stacked bar graph is divided into sub-bars that represent the proportional contribution or contamination factor (C_f) of each element. C_f values determined by using the maximum values of the detection range are marked with asterisks.

4.4. Potential for Metal Release

The results from the short-term leach test conducted to estimate the potential metal release are given in Table 4, along with pH, Eh, and electrical conductivity values, as well as the anion composition (sulfate, nitrate, and chloride) of the leach solutions. The PTE concentrations leached from the soil samples are compared graphically to the total soil contents in Figure 8.

The eluates recovered from the leaching test had pH values equal to or slightly higher than soil pH values (in water). The Technosols PH and LN as well as the sample ZA-1 produced extremely acidic solutions (pH = 2.5–3.5), while the extract solutions from the samples ZA-2 and ZA-3 were moderately acidic (pH = 5.2–5.7). The leachates were characterized by a high redox potential (Eh > 570 mV) with the exception of the sample ZA-3 (Eh = 381 mV). Sulfate was the prevailing anion in all soil extracts, reaching concentrations of up to 652 mg L^{-1} in the sample PH-1. The highest values of electrical conductivity (up to 1.13 mS cm^{-1}) were also observed in the Technosol PH, which is consistent with the water-soluble salt (sulfate) concentration.

Table 4. Physicochemical parameters and trace element concentrations extracted from the Technosols by applying the standard EN-12457-4 leaching test.

| Technosol Sample	pH	Eh mV	CE mS/cm	Sulfate mg/L	Nitrate µg/L	Chloride mg/L	Cr µg/L	Ni µg/L	Cu mg/L	Zn mg/L	As µg/L	Cd µg/L	Pb mg/L
PH-1	3.34	665	0.71	652	440	13	1.6	14.8	5.18	2.25	1.9	37.8	0.05
PH-2	2.50	747	1.13	384	330	1.7	1.1	<0.2	0.23	0.49	3.4	1.8	2.62
PH-3	2.74	731	1.12	618	320	2.4	5.5	7.3	1.43	0.79	7.7	10.4	0.31
ZA-1	3.24	668	0.63	343	540	1.7	1.7	9.2	2.57	2.77	97.5	21.3	0.04
ZA-2	5.18	688	0.03	25	630	1.5	<0.4	2.7	0.14	0.03	0.8	0.2	0.02
ZA-3	5.66	381	0.28	170	560	4.7	<0.4	135.9	55.6	0.79	18.3	36.1	0.02
LN-1	3.07	574	0.49	191	230	6.6	3.2	2.6	0.72	0.04	35.0	0.7	5.55
LN-2	3.22	612	0.59	215	240	1.2	6.9	3.6	0.13	0.24	4.8	3.3	4.36
LN-3	3.54	571	0.18	80	270	2.6	<0.4	<0.2	0.08	0.07	5.1	0.3	9.02
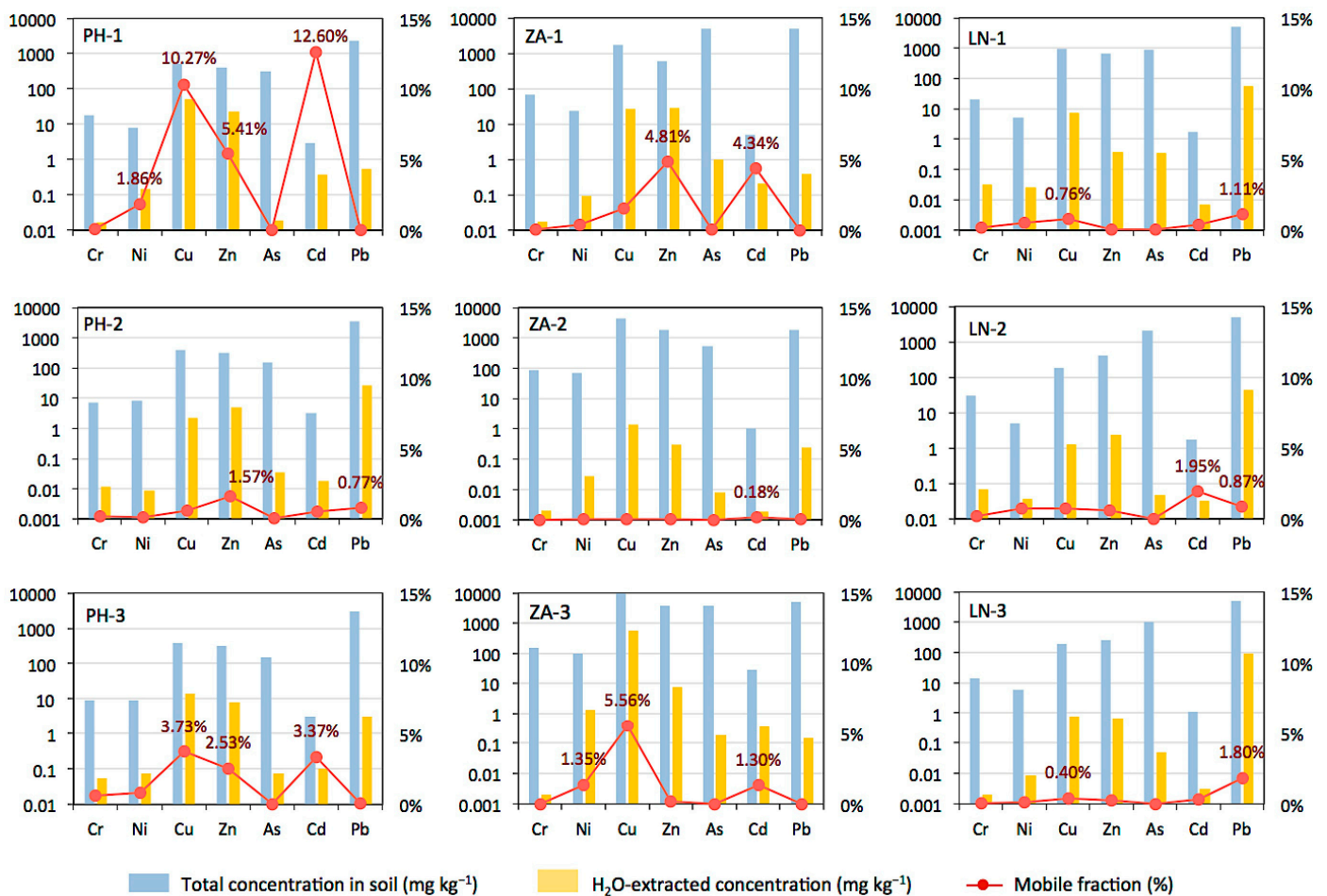
Figure 8. Bar charts comparing the contents of trace elements measured in soil and those measured in leachate (extracted with deionized water), and line charts showing the fraction (%) of metals and metalloids released from the soil (mobile fraction).

The acid leach solutions resulting from the minesoil-water interaction enhanced the solubilization of PTEs to a variable extent, depending on the element involved and the matrix. Copper, Zn, Pb, Cd, and As, in this order of decreasing median concentration, were the most abundant PTEs in the leachates of the Technosols PH and ZA, with peak values of 55.6 mg L^{-1} for Cu (sample ZA-3), 2.25 mg L^{-1} for Zn (sample ZA-1), 2.62 mg L^{-1} for Pb (sample PH-2), 97.5 µg L^{-1} for As (sample ZA-1), and 37.8 µg L^{-1} for Cd (sample PH-1). Interestingly, Pb was released substantially more easily from the Technosol LN,

where pyrite is a ubiquitous phase, with a maximum extraction yield of 9.02 mg L^{-1}. The other PTEs measured in the leachates (Cr and Ni) were found at levels usually below 0.1 mg L^{-1}. The soluble concentrations of Cu and Pb, but also As and Cd, greatly exceeded the safe drinking water standards established in international water quality guidelines (e.g., European Council Directive 98/83/EC and World Health Organization).

In general, the potential metal release from the Technosols when contacted with water is markedly lower in magnitude than that reported for abandoned mine wastes of the Rio Tinto area [45], although Cu and Pb were leached from some soil samples at comparable levels. There are likely to be important contributions of PTEs to surface and shallow groundwater chemistry, which may have an adverse impact on the quality of receiving water bodies. Therefore, in addition to the mine wastes, the mine soils generate drainage that flows into the headwaters of the nearby Tinto River and contributes to its acidification and dissolved metal load.

The samples were classified using a modified Ficklin plot [55] on the basis of the dissolved metal load (sum of Cd, Cu, Ni, Pb, and Zn concentrations) and the pH values of the leach solutions (Figure 9). Most of the samples lie in the acid to high-acid and high-metal to extreme-metal fields, thus showing a hydro-chemical signature similar to that of acid mine waters of the IPB [56–58]. Exceptionally, the sample ZA-3 was classified in the near-neutral extreme-metal class due to the elevated concentration of Cu released into the solution. This can be attributed to the occurrence of soluble hydrated salts that can be easily dissolved under the leach conditions, and serve as a transient pool of available Cu.
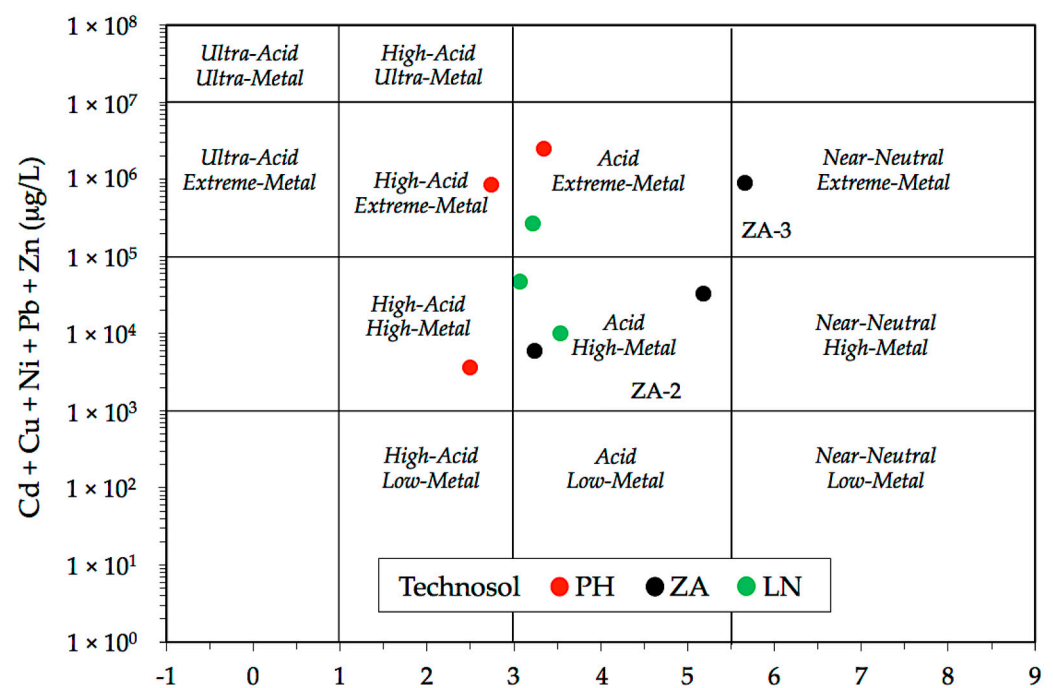

Figure 9. Ficklin diagram plotting the sum of metal concentrations leached from the soil samples against the pH of the leachates.

To further compare the leach test results, the line chart of Figure 8 shows the proportion of the total metal pool that was released from the soil and may be available for plant uptake and leached by percolation. Notwithstanding the high total contents of PTEs occurring in soil, the average values of the water-extractable proportion (Figure 10) were relatively low (less than 5.5%), suggesting that metal mobility was limited for all elements, with maximum release values of 12.60% for Cd and 10.27% for Cu. It is important to note that some of these percentages correspond, nevertheless, to elevated contents of PTEs, which is an issue of concern. The extremely high degree of contamination of the Technosols did

not have a significant correlative effect on the amount of extractable PTEs. This is in good agreement with the results obtained from mine soil samples elsewhere in the IPB [25,59].
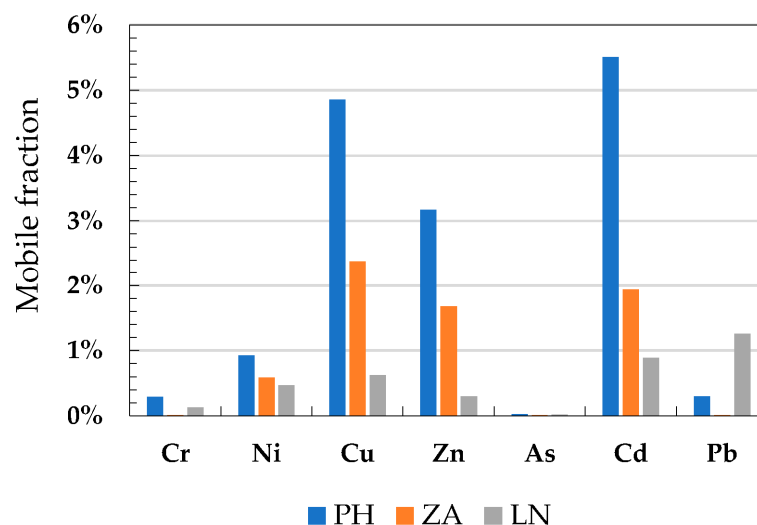

Figure 10. Average values of the trace element fraction extracted from the Technosols by applying the standard EN-12457-4 leaching test.

In most samples PTEs showed the following order of decreasing mobility: Cu > Zn > Cd > Ni > Pb > Cr > As, although Pb was more efficiently leached from the Technosol LN. Accordingly, Cd, Cu, and Zn are the most labile PTEs in mine soils, as they are likely stored in soluble sulfate salts. The fraction of As extracted in the course of the leach test was found to be practically negligible (less than 0.1%), despite the high level of contamination occurring in the Technosols. The low leachability of As with water is consistent with the fact that most of this contaminant could be accommodated by arsenate-for-sulfate substitution in the crystal structure of jarosite [60,61], which is sparingly soluble in water under the acidic and oxidizing conditions prevailing in the mine sites. Besides, the solubility of As could have been limited by adsorption on, or coprecipitation with, iron oxyhydroxide minerals [62] and precipitation of arsenic minerals like scorodite [63], as inferred from the mineralogical analysis. Similarly, the low concentration of Pb in the leach solutions indicated that this heavy metal resides to a large extent in the fixed pool, tightly bonded to soil constituents such as jarosite-like minerals, anglesite, and Pb-bearing phosphate phases. From these findings, it can be arguably claimed that the environmental availability of As and Pb in the short term is very low because, in general, they were not leached abundantly from the mine soils.

According to the aqueous speciation calculations performed using the PHREEQC code [64] with the wateq4f thermodynamic database, the most labile PTEs in soil occurred in the leach solutions in the form of a variety of ionic species (Table 5).

Free metal ion (M^{2+}) was the largely dominant form over the pH range of 2.5 to 5.7, with median values accounting for 100% of dissolved Cd, around 85% of dissolved Cu, Ni, and Zn, and about 70% of dissolved Pb. Sulfate species (MSO_4^0) accounted for most of the remaining species, comprising between 8% and 29% of the median dissolved load of Ni, Cu, Zn, and Pb. Other inorganic complexes such as chloride, nitrate, and hydroxyl ions were not predicted to be significant complexing ligands, because their concentrations in the acid solutions leached from the Technosols were not high enough to be competitive with sulfate ions for PTE speciation. Arsenic release from the soil was present as oxyanion species in the form of arsenate, mainly $H_2AsO_4^-$ and, to a lesser extent, H_3AsO_4. Similar speciation patterns have been reported in previous studies on the modeling of PTE behavior in acidic drainage waters [56,65].

Table 5. Distribution of aqueous species of trace elements of environmental significance in the acid leach solutions indicated as a percent of the total dissolved species.

Element	Species (%)	PH-1	PH-2	PH-3	ZA-1	ZA-2	ZA-3	LN-1	LN-2	LN-3	Median
As	$H_2AsO_4^-$	93.52	65.01	77.15	91.04	100	95.23	86.82	90.53	95.09	91.04
	$HAsO_4^{2-}$						4.77				
	H_3AsO_4	6.48	34.99	22.85	8.96			13.18	9.47	4.91	8.96
Cd	Cd^{2+}	100	100	100	100	100	100	100	100	100	100
Cu	Cu^{2+}	90.29	75.31	82.04	73.28	96.26	93.59	82.76	86.57	89.49	86.57
	$CuSO_4$	9.68	24.69	17.95	26.71	3.61	5.58	17.21	13.43	10.51	13.43
	$CuOH^+$					0.13	0.28				
	$Cu(OH)_2$						0.22				
	$CuCl^+$	0.03		0.01	0.01		0.02	0.03			0.01
	$Cu_2(OH)_2^{2+}$						0.32				
Ni	Ni^{2+}	91.32		83.42	74.71	96.58	94.86	83.68	87.4		83.68
	$NiSO_4$	8.68		16.58	25.29	3.42	5.14	16.32	12.6		8.68
Pb	Pb^{2+}	77.33	51.49	62.29	48.79	90.44	86.15	62.89	69.81	74.66	69.81
	$PbSO_4$	21.87	47.53	36.87	50.18	9.56	13.85	36.4	29.84	25.06	29.84
	$PbCl^+$	0.44	0.06	0.09				0.34	0.06	0.17	0.06
	$Pb(SO_4)_2^{2-}$	0.36	0.91	0.75	1.03			0.37	0.28	0.12	0.36
Zn	Zn^{2+}	88.78	72.13	79.45	69.91	95.86	93.52	80.5	84.72	88.09	84.72
	$ZnSO_4$	10.9	27.02	19.9	29.12	4.11	6.38	19.17	15.05	11.82	15.05
	$ZnOH^+$					0.01	0.02				
	$Zn(SO_4)_2^{2-}$	0.29	0.84	0.64	0.97	0.01	0.05	0.31	0.22	0.09	0.29
	$ZnCl^+$	0.03		0.01	0.01	0.01	0.02	0.03			0.01

The leach solutions from the Technosol ZA displayed a more complex speciation pattern. The activity of sulfate species decreased noticeably with increasing pH from 3.2 (sample ZA-1) to 5.7 (sample ZA-3), while the contribution of hydroxyl complexes of Cu and Zn in the aqueous solution was shown to increase, although to a still relatively very low level. Therefore, the distribution of major species seems to be related to the solution pH.

The saturation index (SI) values for solid phases were computed with PHREEQC by comparing measured solution activity, expressed as an ion activity product (IAP) with the theoretical solubility product constant (Ksp), as follows:

$$SI = log\left(\frac{IAP}{K_{sp}}\right)$$

The geochemical modeling approach of the mine soil-water interaction indicated a slight supersaturation with respect to anglesite (SI = 0.16–0.21) in the Technosol LN, which is consistent with the observed mineralogy, and also with copper-rich secondary minerals, like brochantite (SI = 2.15) and antlerite (SI = 1.19), that may form from evaporation at the site ZA-3. The extracts were undersaturated (SI < 0) with all the Cd- and Zn-bearing minerals in the database, so it is unlikely that such phases are present as precipitates under the prevailing conditions.

5. Conclusions

This paper has highlighted the importance of determining the various forms of acidity and the potential for the release and mobilization of PTEs at historically contaminated mine sites in order to assess the risk of water contamination by leaching through the soil. Specifically, it has been shown that soils contaminated with hazardous mine waste at Rio Tinto have become secondary source areas of acidic effluents and harmful contaminants to the surrounding environment. These soils have a remarkable acid-production capacity due to sulfide oxidation and an existing acidity, albeit often neglected, that may be slowly released by hydrolysis of jarosite-like minerals. It was also found that they contain anomalous

contents of As, Pb, Cu, and Zn, mostly linked to heavy metal-bearing particles inherited from the wasteland, but also structurally bound in soil-forming minerals thus limiting their environmental significance. Notwithstanding, there still is a persistent reservoir of readily leachable Cu, Cd, Zn, and Pb, in the form of free metal ions and sulfate species that are being flushed into the Tinto River system. The extreme acidity and metal release will likely be maintained over time due to the occurrence of actively oxidizing pyrite. Ultimately, in light of these findings, an effective mine land reclamation program should not be limited to abandoned mine wastes but should also ensure that acidity and metal mobility in the mining-affected soils are reduced to environmentally sustainable levels.

Supplementary Materials: The following supporting information can be downloaded at: https://www.mdpi.com/article/10.3390/min13040456/s1, Table S1: ICP-OES and ICP-MS operating conditions.

Author Contributions: S.F.-L.: investigation; formal analysis; data curation; software; visualization; writing-original draft preparation. J.C.F.-C.: investigation; conceptualization; methodology; visualization; validation; original draft preparation; supervision; project administration; M.I.G.: investigation; formal analysis; methodology; validation; writing-review and editing; resources. E.M.: investigation; formal analysis; validation; writing-review and editing. C.B.-B.: investigation; formal analysis; validation; writing-review and editing. I.G.: investigation; formal analysis; validation; writing-review and editing. All authors have read and agreed to the published version of the manuscript.

Data Availability Statement: The authors confirm that the data supporting the findings of this study are available within the manuscript.

Conflicts of Interest: The authors declare no conflict of interest.

Abbreviations

ABA: Acid-Base Accounting. AMD: Acid Mine Drainage. ASD: Acid Soil Drainage. ASTM: American Standard Test Method. BSE: Back Scattered Electron. EC: Electrical Conductivity. EDS: Energy Dispersive X-ray Spectroscopy. EPMA: Electron Probe Micro Analysis. FESEM: Field-Emission Scanning Electron Microscopy. ICP-MS: Inductively Coupled Plasma Mass Spectrometry. ICP-OES: Inductively Coupled Plasma Optical Emission Spectrometry. IPB: Iberian Pyrite Belt. ISO: International Organization for Standardization. IUSS: International Union of Soil Sciences. NAG: Net Acid Generation. PLI: Pollution Load Index. PSA: Potential Sulfidic Acidity. PTE: Potentially Toxic Trace Elements. RA: Retained Acidity. RSD: Relative Standard Deviation. RTC: Rio Tinto Company. SE: Secondary Electron. SI: Saturation Index. TAA: Titratable Actual Acidity. TAG: Total Acid Generation. VMS: Volcanogenic Massive Sulfide. WRB: World Reference Base. XRD: X-ray Diffraction.

References

1. Salomons, W. Environmental impact of metals derived from mining activities. *J. Geochem. Explor.* **1995**, *53*, 53–56.
2. Nordstrom, D.K. Hydrogeochemical processes governing the origin, transport and fate of major and trace elements from mine wastes and mineralized rock to surface waters. *Appl. Geochem.* **2011**, *26*, 1777–1791. [CrossRef]
3. Hudson-Edwards, K. Tackling mine wastes. *Science* **2016**, *352*, 288–290. [CrossRef]
4. Plumlee, G.S.; Morman, S.A. Mine wastes and human health. *Elements* **2011**, *7*, 399–404. [CrossRef]
5. Sánchez de la Campa, A.; De la Rosa, J.D.; Fernández-Caliani, J.C.; González-Castanedo, Y. Impact of abandoned mine waste on atmospheric respirable particulate matter in the historic mining district of Rio Tinto (Iberian Pyrite Belt). *Environ. Res.* **2011**, *111*, 1018–1023. [CrossRef] [PubMed]
6. Castillo, S.; De la Rosa, J.; Sánchez de la Campa, A.; González-Castanedo, Y.; Fernández-Caliani, J.C.; González, I.; Romero, A. Contribution of mine wastes to atmospheric metal deposition in the surrounding area of an abandoned heavily polluted mining district (Rio Tinto mines, Spain). *Sci. Total Environ.* **2013**, *449*, 363–372. [CrossRef] [PubMed]
7. Romero, A.; González, I.; Martín, J.M.; Vázquez, M.A.; Ortiz, P. Risk assessment of particle dispersion and trace element contamination from mine-waste dumps. *Environ. Geochem. Health* **2015**, *37*, 273–286. [CrossRef]

8. Helser, J.; Vassilieva, E.; Cappuyns, V. Environmental and human health risk assessment of sulfidic mine waste: Bioaccessibility, leaching and mineralogy. *J. Hazard. Mat.* **2022**, *424*, 127313. [CrossRef]

9. Jambor, J.L. Mine-waste mineralogy and mineralogical perspectives of acid-base accounting. In *Environmental Aspects of Mine Wastes*; Jambor, J.L., Blowes, D.W., Ritchie, A.I.M., Eds.; Mineralogical Association of Canada Short Course: Ottawa, ON, Canada, 2003; Volume 31, pp. 117–146.

10. Lottermoser, B.G. Mine Wastes. In *Characterization, Treatment and Environmental Impacts*, 3rd ed.; Springer: Berlin/Heidelberg, Germany, 2010.

11. Jamieson, H.E.; Stephen, S.R.; Parsons, M.B. Mineralogical characterization of mine waste. *Appl. Geochem.* **2015**, *57*, 85–105. [CrossRef]

12. Cánovas, C.R.; De La Aleja, C.G.; Macías, F.; Pérez-López, R.; Basallote, M.D.; Olías, M.; Nieto, J.M. Mineral reactivity in sulphide mine wastes: Influence of mineralogy and grain size on metal release. *Eur. J. Mineral.* **2019**, *31*, 263–273. [CrossRef]

13. Arranz, J.C.; Rodríguez-Gómez, V.; Fernández-Naranjo, F.J.; Vadillo, L. Assessment of the pollution potential of a special case of abandoned sulfide tailings impoundment in Riotinto mining district (SW Spain). *Environ. Sci. Pollut. Res.* **2021**, *28*, 14054–14067. [CrossRef]

14. IUSS Working Group WRB. World Reference Base for Soil Resources 2014. In *International Soil Classification System for Naming Soils and Creating Legends for Soil Maps, Update 2015*; World Soil Resources Reports; FAO: Rome, Italy, 2015; Volume 106, pp. 1–192.

15. Gómez-González, M.A.; Voegelin, A.; García-Guinea, J.; Bolea, E.; Laborda, F.; Garrido, F. Colloidal mobilization of arsenic from mining-affected soils by surface runoff. *Chemosphere* **2016**, *144*, 1123–1131. [CrossRef] [PubMed]

16. Hudson-Edwards, K.A.; Schell, C.; Macklin, M.G. Mineralogy and geochemistry of alluvium contaminated by metal mining in the Rio Tinto area, southwest Spain. *Appl. Geochem.* **1999**, *14*, 1015–1030. [CrossRef]

17. García-Palomero, F. Mineralizaciones de Riotinto (Huelva): Geología, génesis y modelos geológicos para su explotación y evaluación de reservas minerales. In *Recursos Minerales de España*; Martínez-Frías, J., García-Guinea, J., Eds.; Consejo Superior de Investigaciones Científicas, Textos Universitarios: Madrid, Spain, 1992; Volume 15, pp. 1325–1352.

18. Noble, A.C. Technical Report on the Riotinto Copper Project. 2022. Available online: https://atalayamining.com/wp-content/uploads/2022/09/Technical-Report-on-the-Riotinto-Project_Sept2022_FINAL.pdf (accessed on 2 February 2023).

19. De Mello, C.R.; Tornos, F.; Conde, C.; Tassinari, C.C.G.; Farci, A.; Vega, R. Geology, geochemistry, and geochronology of the giant Rio Tinto VMS deposit, Iberian Pyrite Belt, Spain. *Econ. Geol.* **2022**, *117*, 1149–1177. [CrossRef]

20. Dutrizac, J.E.; Jambor, J.L.; O'Reilly, J.B. Man's first use of jarosite: The pre-Roman mining-metallurgical operations at Rio Tinto, Spain. *Can. Min. Metall. Bull.* **1983**, *76*, 78–82.

21. Rothenberg, B.; García-Palomero, F. The Rio Tinto enigma-no more. *Inst. Archaeo-Metall. Stud. Newsl.* **1986**, *8*, 3–5.

22. Salkield, L.U. *A Technical History of the Rio Tinto Mines: Some Notes on Exploitation from Pre-Phoenician Times to the 1950s*; The Institution of Mining and Metallurgy: London, UK, 1987; p. 116.

23. Gallego, L.; Fernández-Caliani, J.C. Pyrite ore cargo spills as a source of soil pollution and ecological risk along the abandoned railway corridors of the Tharsis and Rio Tinto mines (Spain). *Environ. Monit. Assess.* **2023**, *195*, 97. [CrossRef] [PubMed]

24. Lottermoser, B.G. Evaporative mineral precipitates from a historical smelting slag dump, Rio Tinto, Spain. *Neues Jb. Miner. Abh.* **2005**, *181*, 183–190. [CrossRef]

25. Chopin, E.I.B.; Alloway, B.J. Trace element partitioning and soil particle characterisation around mining and smelting areas at Tharsis, Riotinto and Huelva, SW Spain. *Sci. Total Environ.* **2007**, *373*, 488–500. [CrossRef] [PubMed]

26. López, M.; González, I.; Romero, A. Trace element contamination of agricultural soils affected by sulphide exploitation (Iberian Pyrite Belt, SW Spain). *Environ. Geol.* **2008**, *54*, 805–818. [CrossRef]

27. Fernández-Caliani, J.C.; Barba-Brioso, C.; González, I.; Galán, E. Heavy metal pollution in soils around the abandoned mine sites of the Iberian Pyrite Belt (Southwest Spain). *Water Air Soil Pollut.* **2009**, *200*, 211–226. [CrossRef]

28. González, I.; Galán, E.; Romero, A. Assessing soil quality in areas affected by sulfide mining. Application to soils in the Iberian Pyrite Belt (SW Spain). *Minerals* **2011**, *1*, 73–108. [CrossRef]

29. Arranz, J.C.; Cala, V.; Iribarren, I. Geochemistry and mineralogy of surface pyritic tailings impounds at two mining sites of the Iberian Pyrite Belt (SW Spain). *Environ. Earth Sci.* **2012**, *65*, 669–680. [CrossRef]

30. Romero-Baena, A.J.; Barba-Brioso, C.; Ross, A.; González, I.; Aparicio, P. Mobility of potentially toxic elements in family garden soils of the Riotinto mining area. *Appl. Clay Sci.* **2021**, *203*, 105999. [CrossRef]

31. Urrutia, M.M.; García-Rodeja, E.; Macias, F. Sulfide oxidation in coal-mine dumps: Laboratory measurement of acidifying potential with H_2O_2 and its application to characterize spoil materials. *Environ. Manag.* **1992**, *16*, 81–89. [CrossRef]

32. Kahle, M.; Kleber, M.; Jahn, R. Review of XRD-based quantitative analyses of clay minerals in soils: The suitability of mineral intensity factors. *Geoderma* **2002**, *109*, 191–205. [CrossRef]

33. Bussan, D.; Harris, A.; Douvris, C. Monitoring of selected trace elements in sediments of heavily industrialized areas in Calcasieu Parish, Louisiana, United States by inductively coupled plasma-optical emission spectroscopy (ICP-OES). *Microchem. J.* **2019**, *144*, 51–55. [CrossRef]

34. Ahern, C.R.; McElnea, A.E.; Sullivan, L.A. *Acid Sulfate Soils Laboratory Methods Guidelines*; Queensland Department of Natural Resources, Mines and Energy: Indooroopilly, Australia, 2004.

35. Nordstrom, D.K. Aqueous pyrite oxidation and the consequent formation of secondary iron minerals. In *Acid Sulfate Weathering*; Kittrick, J.A., Fanning, D.S., Hossner, L.R., Eds.; SSSA Special Publications; Soil Science Society of America: Madison, WI, USA, 1982; Volume 10, pp. 37–56.

36. Dold, B. Acid rock drainage prediction: A critical review. *J. Geochem. Explor.* **2017**, *172*, 120–132. [CrossRef]
37. McElnea, A.E.; Ahern, C.R.; Menzies, N.W. The measurement of actual acidity in acid sulfate soils and the determination of sulfidic acidity in suspension after peroxide oxidation. *Austr. J. Soil Res.* **2002**, *40*, 1133–1157. [CrossRef]
38. Dold, B. Speciation of the most soluble phases in a sequential extraction procedure adapted for geochemical studies of copper sulfide mine waste. *J. Geochem. Explor.* **2003**, *80*, 55–68. [CrossRef]
39. *EN 12457-2:2002*; European Standard EN 12457-2 Characterization of Waste–Leaching–Compliance Test for Leaching of Granular Waste Materials and Sludges, Part 2: One Stage Batch Test at a Liquid to Solid Ratio of 10 l/kg for Materials with Particle Size below 4 mm (without or with Size Reduction). European Committee for Standardization: Brussels, Belgium, 2002.
40. López-Arce, P.; Garrido, F.; García-Guinea, J.; Voegelin, A.; Göttlicher, J.; Nieto, J.M. Historical roasting of thallium- and arsenic-bearing pyrite: Current Tl pollution in the Riotinto mine area. *Sci. Total Environ.* **2019**, *648*, 1263–1274. [CrossRef]
41. Romero, A.; González, I.; Galán, E. Estimation of potential pollution of waste mining dumps at Peña del Hierro (Pyrite Belt, SW Spain) as a base for future mitigation actions. *Appl. Geochem.* **2006**, *21*, 1093–1108. [CrossRef]
42. Jerz, J.K.; Rimstidt, J.D. Efflorescent iron sulfate minerals: Paragenesis, relative stability, and environmental impact. *Am. Miner.* **2003**, *88*, 1919–1932. [CrossRef]
43. Miller, S.; Robertson, A.; Donahue, T. Advances in acid drainage prediction using the net acid generating (NAG) test. In Proceedings of the fourth International Conference on Acid Rock Drainage, Vancouver, BC, Canada, 31 May–6 June 1997; Volume 2, pp. 533–547.
44. Karlsson, T.; Räisänen, M.L.; Lehtonen, M.; Alakangas, L. Comparison of static and mineralogical ARD prediction methods in the Nordic environment. *Environ. Monit. Assess.* **2018**, *190*, 719. [CrossRef] [PubMed]
45. Cánovas, C.R.; Quispe, D.; Macías, F.; Callejón-Leblic, B.; Arias-Borrego, A.; García-Barrera, T.; Nieto, J.M. Potential release and bioaccessibility of metal/loids from mine wastes deposited in historical abandoned sulfide mines. *Environ. Pollut.* **2023**, *316*, 120629. [CrossRef]
46. Li, Z.; Ma, Z.; Van der Kuijp, T.J.; Yuan, Z.; Huang, L. A review of soil heavy metal pollution from mines in China: Pollution and health risk assessment. *Sci. Total Environ.* **2014**, *468–469*, 843–853. [CrossRef] [PubMed]
47. Barsova, N.; Yakimenko, O.; Tolpeshta, I.; Motuzova, G. Current state and dynamics of heavy metal soil pollution in Russian Federation—A review. *Environ. Pollut.* **2019**, *249*, 200–207. [CrossRef] [PubMed]
48. Reimann, C.; Caritat, P. *Chemical Elements in the Environment*; Springer: Berlin/Heidelberg, Germany, 1998; p. 398.
49. Grantcharova, M.M.; Fernández-Caliani, J.C. Soil acidification, mineral neoformation and heavy metal contamination driven by weathering of sulphide wastes in a Ramsar wetland. *Appl. Sci.* **2022**, *12*, 249. [CrossRef]
50. Galán, E.; Fernández Caliani, J.C.; González, I.; Aparicio, P.; Romero, A. Influence of geological setting on geochemical baselines of trace elements in soils. Application to soils of South-West Spain. *J. Geochem. Explor.* **2008**, *98*, 89–106. [CrossRef]
51. Fernández-Caliani, J.C. La contaminación del suelo por la minería metálica de la Faja Pirítica Ibérica. *Macla* **2022**, *26*, 1–2.
52. Hakanson, L. An ecological risk index for aquatic pollution control: A sedimentological approach. *Water Res.* **1980**, *14*, 975–1001. [CrossRef]
53. Tomlinson, D.L.; Wilson, J.G.; Harris, C.R.; Jeffrey, D.W. Problems in the assessment of heavy-metal levels in estuaries and the formation of a pollution index. *Helgol. Meeresunters.* **1980**, *33*, 566–575. [CrossRef]
54. Abrahim, G.M.S.; Parker, R.J. Assessment of heavy metal enrichment factors and the degree of contamination in marine sediments from Tamaki Estuary, Auckland, New Zealand. *Environ. Monit. Assess.* **2007**, *136*, 227–238. [CrossRef] [PubMed]
55. Ficklin, W.H.; Plumlee, G.S.; Smith, K.S.; McHugh, J.B. Geochemical classification of mine drainages and natural drainages in mineralized areas. In Proceedings of the 7th International Symposium on Water-Rock Interaction, Park City, UT, USA, 13–18 July 1992; pp. 381–384.
56. Sánchez-España, J.; López-Pamo, E.; Santofimia, E.; Aduvire, O.; Reyes-Andrés, J.; Barettino, D. Acid mine drainage in the Iberian Pyrite Belt (Odiel river watershed, Huelva, SW Spain): Geochemistry, mineralogy and environmental implications. *Appl. Geochem.* **2005**, *20*, 1320–1356. [CrossRef]
57. Romero, A.; González, I.; Galán, E. Stream water geochemistry from mine wastes in Peña de Hierro, Riotinto Area, SW Spain. A case of extreme acid mine drainage. *Environ. Earth Sci.* **2011**, *62*, 645–656. [CrossRef]
58. Durães, N.; Bobos, I.; Ferreira da Silva, E. Speciation and precipitation of heavy metals in high-metal and high-acid mine waters from the Iberian Pyrite Belt (Portugal). *Environ. Sci. Pollut. Res.* **2017**, *24*, 4562–4576. [CrossRef] [PubMed]
59. Madejón, P.; Barba-Brioso, C.; Lepp, N.W.; Fernández-Caliani, J.C. Traditional agricultural practices enable sustainable remediation of highly polluted soils in Southern Spain for cultivation of food crops. *J. Environ. Manag.* **2011**, *92*, 1828–1836. [CrossRef]
60. Paktunc, D.; Dutrizac, J.E. Characterization of arsenate-for-sulfate substitution in synthetic jarosite using X-ray diffraction and X-ray absorption spectroscopy. *Canad. Mineral.* **2003**, *41*, 905–919. [CrossRef]
61. Asta, M.P.; Cama, J.; Martínez, M.; Giménez, J. Arsenic removal by goethite and jarosite in acidic conditions and its environmental implications. *J. Hazard. Mater.* **2009**, *171*, 965–972. [CrossRef]
62. Morin, G.; Calas, G. Arsenic in soils, mine tailings, and former industrial sites. *Elements* **2006**, *2*, 97–101. [CrossRef]
63. Haffert, L.; Craw, D. Mineralogical controls on environmental mobility of arsenic from historic mine processing residues, New Zealand. *Appl. Geochem.* **2008**, *23*, 1467–1483. [CrossRef]

64. Parkhurst, D.L.; Appelo, C.A.J. Description of input and examples for PHREEQC version 3—A computer program for speciation, batch-reaction, one-dimensional transport, and inverse geochemical calculations. *US Geol. Surv. Tech. Methods* **2013**, *6*, 497.
65. Plumlee, G.S.; Smith, K.S.; Montour, M.R.; Ficklin, W.H.; Mosier, E.L. Geologic controls on the composition of natural waters and mine waters draining diverse mineral–deposit types. In *The Environmental Geochemistry of Mineral Deposits. Part B: Case Studies and Research Topics*; Filipek, L.H., Plumlee, G.S., Eds.; Reviews in Economic Geology; Society of Economic Geologists: Littleton, CO, USA, 1999; Volume 6B, pp. 373–432.